

Visco-Poroelastic Electrochemiluminescence Skin with Piezo-Ionic Effect

Jong Ik Lee, Hanbin Choi, Seok Hwan Kong, Sangsik Park, Dongmok Park, Joo Sung Kim, Sung Hyun Kwon, Jungwook Kim, Soo Hyung Choi, Seung Geol Lee, **Do Hwan Kim**,* and Moon Sung Kang*

Following early research efforts devoted to achieving excellent sensitivity of electronic skins, recent design schemes for these devices have focused on strategies for transduction of spatially resolved sensing data into straightforward user-adaptive visual signals. Here, a material platform capable of transducing mechanical stimuli into visual readout is presented. The material layer comprises a mixture of an ionic transition metal complex luminophore and an ionic liquid (capable of producing electrochemiluminescence (ECL)) within a thermoplastic polyurethane matrix. The proposed material platform shows visco-poroelastic response to mechanical stress, which induces a change in the distribution of the ionic luminophore in the film, which is referred to as the piezo-ionic effect. This piezo-ionic effect is exploited to develop a simple device containing the composite layer sandwiched between two electrodes, which is termed “ECL skin”. Emission from the ECL skin is examined, which increases with the applied normal/tensile stress. Additionally, locally applied stress to the ECL skin is spatially resolved and visualized without the use of spatially distributed arrays of pressure sensors. The simple fabrication and unique operation of the demonstrated ECL skin are expected to provide new insights into the design of materials for human–machine interactive electronic skins.

1. Introduction

The recent emergence of soft electronics has led to the realization of devices that can not only withstand gentle flexing but also undergo stronger deformation, for example, rolling and stretching.^[1–3] The task of interfacing such technology with humans or robots has opened up avenues for the development of an unprecedented wearable device platform known as electronic skin.^[4–6] Electronic skin is a multimodal network of electronic sensors with mechanical deformability, which enables the perception of various external stimuli, such as, mechanical, chemical, thermal, and optical stimuli.^[1,7–10] After early efforts aimed at the development of electronic skins with excellent sensitivity, later design efforts for these devices have been concentrated on the transduction of spatially resolved sensing data into the most straightforward readout, that is, visual signals. For example, Javey

J. I. Lee, D. Park, Prof. J. Kim
 Department of Chemical and Biomolecular Engineering
 Sogang University
 Seoul 04107, Republic of Korea

H. Choi, J. S. Kim
 Department of Chemical Engineering
 Hanyang University
 Seoul 04763, Republic of Korea

S. H. Kong
 Department of Chemical Engineering
 Soongsil University
 Seoul 06978, Republic of Korea

S. Park
 Department of Organic Materials and Fiber Engineering
 Soongsil University
 Seoul 06978, Republic of Korea

S. H. Kwon
 Department of Organic Material Science and Engineering
 Pusan National University
 Busan 46241, Republic of Korea

Prof. S. H. Choi
 Department of Chemical Engineering
 Hongik University
 Seoul 04066, Republic of Korea

Prof. S. G. Lee
 School of Chemical Engineering
 Department of Organic Material Science and Engineering
 Pusan National University
 Busan 46241, Republic of Korea

Prof. D. H. Kim
 Department of Chemical Engineering
 Institute of Nano Science and Technology
 Hanyang University
 Seoul 04763, Republic of Korea
 E-mail: dhkim76@hanyang.ac.kr

Prof. M. S. Kang
 Department of Chemical and Biomolecular Engineering
 Institute of Emergent Materials
 Sogang University
 Seoul 04107, Republic of Korea
 E-mail: kangms@sogang.ac.kr



The ORCID identification number(s) for the author(s) of this article can be found under <https://doi.org/10.1002/adma.202100321>.

DOI: 10.1002/adma.202100321

et al.^[11] integrated an active-matrix organic light-emitting device (OLED) display onto an elastomeric substrate and connected the electrodes to a pressure-sensitive rubbery conductor. Local pressure applied to the resulting electronic-skin device could be spatially resolved and visually displayed on a pixel scale, which, as a consequence, could be quantified in terms of the local light intensity. This result motivated exploitation of pressure-sensitive device components (e.g., gate dielectrics,^[12] integrated units,^[13] and electrodes^[14]) within OLEDs. Fabrication of these devices necessitates integration of functional elements, including arrays of pressure sensors, display units, and driving units, which is a complicated task. Wang et al.^[15] utilized the unique property of ZnO/GaN nanowire light-emitting diodes (LEDs), that is, local strain- or pressure-dependent emission, termed the piezo-phototronic effect, for transducing mechanical stress into visible readout. Electronic skin realized using an array of such piezo-phototronic nanowires enabled 2D mapping of the distribution of pressure applied to the skin on a micrometer scale. In these devices, pressure sensing and visual readout are performed using the same electronic component. However, realization of these device structures inevitably involves complicated fabrication procedures for the arrays of such nanostructured components.

Recently, simpler device structures have been developed for translating mechanical stimuli into visual signals. For example, ruthenium complexes embedded in porous matrix were

exploited for pressure-sensitive paints. There, the permeability of the matrix to oxygen varied sensitively with applied pressure, leading to pressure-dependent quenching in the photoluminescence from the complexes.^[16–18] Triboelectric charge generation was also used as a driving scheme to induce transient emission from phosphores placed on a spatially resolved passive matrix.^[19,20] Phosphores confined in a stretchable network, serving as a capacitor-type AC-driven luminescence layer, could be utilized for visualizing tactile stimuli.^[21–23] Pressure applied to the device changed the thickness of the luminescence layer and eventually the intensity of the light emission. Despite the simplicity of this phosphore-based device structure, such devices require operation voltages higher than 1 kV. Therefore, an alternative electronic-skin structure is highly desirable that can be fabricated by a simple method, operate at practical voltages, and have high sensitivity and a good spatial resolution under exposure to mechanical stimuli.

Examples of transduction of mechanical stimuli into visual readout can be found in nature; this phenomenon is also an interesting motif for the design of a simpler device scheme. For example, dinoflagellates, tiny unicellular phytoplankton found in the ocean, produce flow-stimulated bioluminescence and scintillate like stars in the sky in the dark (Figure 1a). The full mechanotransduction process in dinoflagellates is not yet completely understood, but it is known that the shear force acting on the cells promotes intracellular Ca^{2+} flux in the cytoplasm

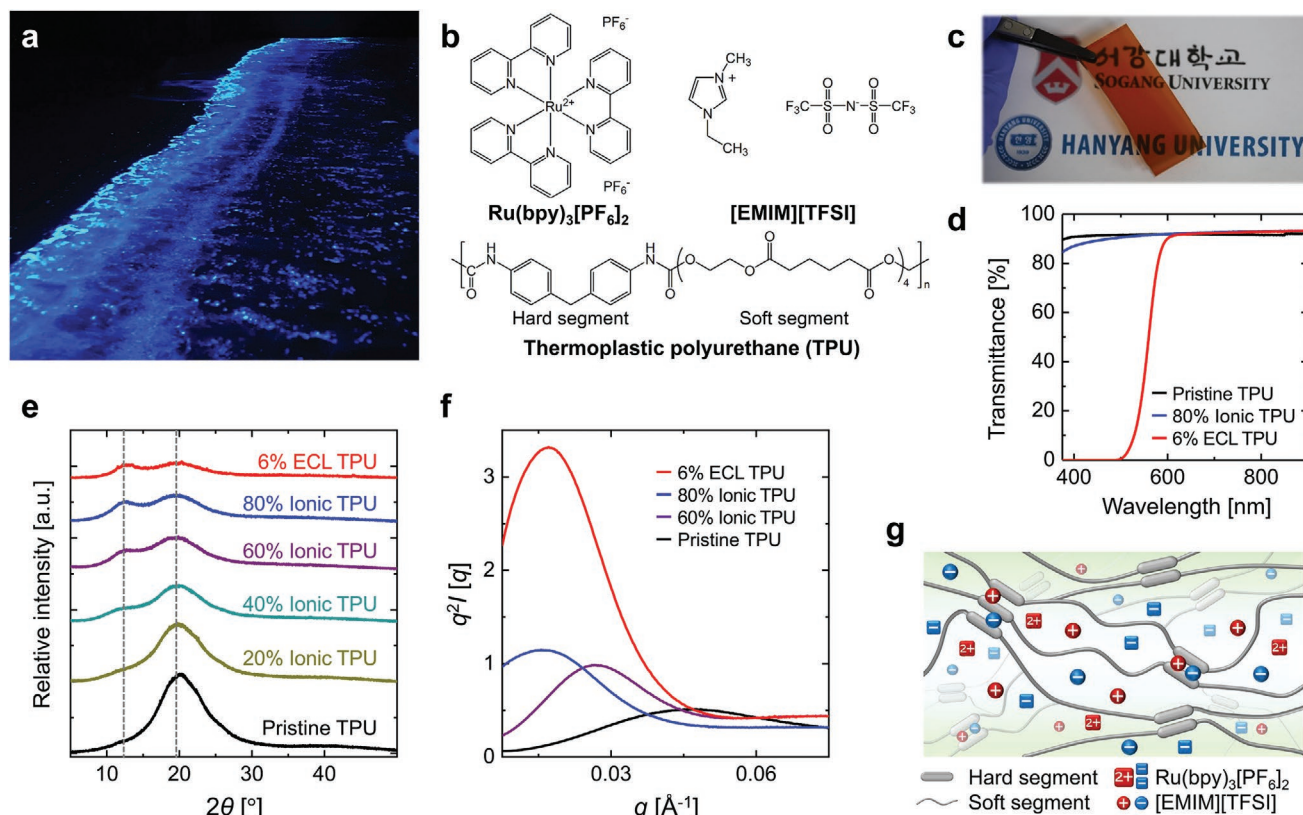


Figure 1. a) Photograph of flow-stimulated bioluminescence from dinoflagellates near seashore. b) Chemical structures of three critical constituents (ECL luminophore, IL, and matrix polymer) of active composite layer of ECL TPU film. c) Photograph of transparent ECL TPU film (6 wt%). d) Optical transmittance spectra of pristine TPU film, ionic TPU film (80 wt%), and ECL TPU film (6 wt%). e) XRD and f) SAXS patterns of pristine TPU film, ionic TPU films with different contents of IL, and ECL TPU. g) Schematic depiction of microscopic structure of ECL TPU film.

and eventually activates the luminescent chemistry.^[24–26] The electrochemical reaction in this process requires a potential no higher than 1 V. Inspired by this motif, we devise a scheme for a simple, deformable electronic skin device that transduces local stress into a spatially resolved light signal by an electrochemical process involving ions. The emissive layer of our electronic skin is made of a physically crosslinked polymer matrix swelled with a mixture of an ionic transition metal complex (iTMC) and an ionic liquid (IL). The included ionic mixture can exhibit electrochemically generated chemiluminescence or electrochemiluminescence (ECL), as a consequence of a charge transfer reaction between the oxidized and reduced forms of the iTMC.^[27,28] See Supporting Information for brief description of ECL process we exploited. We note that for these devices based on ECL, charges are typically transferred by convective process (which involves direct mass transfer for oxidized and reduced iTMC species),^[27] whereas charges in their sister electrochemical devices, often referred to as the light-emitting electrochemical cells,^[29] charge are transferred by conductive process (which involves hopping of electrons and holes through iTMCs). Our developed device is hereafter referred to as “ECL skin”. The polymer matrix enables the device to be both flexible and stretchable. More importantly, the tough gel network can undergo visco-poroelastic relaxation under applied stress. That is, any mechanical stress applied to the composite layer is relieved via adjustment of the conformation of the matrix polymer (viscoelastic relaxation) and/or a change in the nanoscale free volume of the matrix (poroelastic relaxation). A combination of these two effects facilitates a change in the distribution of the ionic ECL mixture embedded in the scaffolding matrix, which we refer as the piezo-ionic effect.^[30] The piezo-ionic effect, in turn, results in an enhancement of the luminescence intensity. The luminescence intensity of the device is confirmed to vary systematically with both normal and tensile stresses. Because visco-poroelastic relaxation of the polymer matrix occurs only at the location where stress is applied, the tactile stimulus can be spatially mapped without the use of complicated driving schemes. We believe that the device concept demonstrated herein can provide new approaches for the design of low-power, mechanosensitive photonic skin capable of transducing mechanical stimuli into direct visual outputs.

2. Results and Discussion

Figure 1b shows the chemical structures of the three critical components constituting the active composite layer of our ECL skin device. Tris(2,2'-bipyridine)ruthenium(II) hexafluorophosphate ($[\text{Ru}(\text{bpy})_3][\text{PF}_6]_2$) is used as the ECL luminophore, and the 1-ethyl-3-methylimidazolium bis(trifluoromethanesulfonyl) imide ($[\text{EMIM}]^+[\text{TFSI}]^-$) is used as the IL electrolyte necessary for inducing the electrochemical reaction. A thermoplastic polyurethane (TPU) random copolymer containing a methylene diphenyl diisocyanate hard segment and a polyadipate soft segment is used as the elastomeric matrix.^[31] ECL occurs upon the relaxation of the excited luminophore ($[\text{Ru}(\text{bpy})_3]^{2+*}$) formed via the charge transfer reaction between the reduced species ($[\text{Ru}(\text{bpy})_3]^{1+}$) and the oxidized species ($[\text{Ru}(\text{bpy})_3]^{3+}$).^[27,28,32] The use of a nonvolatile IL electrolyte with a large electrochemical

window is critical for ensuring device operation without an undesirable Faradaic reaction of the electrolyte.^[33] Spin coating of a 1:16:4 (wt%) mixture of $[\text{Ru}(\text{bpy})_3][\text{PF}_6]_2$, $[\text{EMIM}]^+[\text{TFSI}]^-$, TPU dissolved in a dimethylformamide solvent, and a subsequent drying process yield a self-standing, tough composite film, denoted as the ECL TPU film (Figure 1c). The transparency of the ECL TPU indicates the homogeneous nature of the composite film (Figure 1d).

The microstructures of a series of composite films were analyzed using combinatorial X-ray analysis, that is, X-ray diffraction (XRD) and small-angle X-ray scattering (SAXS). Figure 1e and Figure S1, Supporting Information, show the XRD patterns of the following: a pristine TPU film; TPU composite films with different contents of the IL ($[\text{EMIM}]^+[\text{TFSI}]^-$), hereafter referred to as ionic TPU films and the TPU film containing both the luminophore and the IL, that is, the ECL TPU film. The black curve is a diffractogram obtained from the pristine TPU film. The hard segment of the TPU polymer forms well-organized domains that can serve as a physical crosslinking point of the gel network, whereas the soft segment constitutes the nanoscale free volume of the gel network (this is discussed in detail later). The XRD peak at 19.3° (d -spacing: 4.5 \AA) confirms the formation of well-organized domains of hard segments in the pristine TPU film. The IL ($[\text{EMIM}]^+[\text{TFSI}]^-$) added to the TPU functions as a plasticizer. In such a composite material (i.e., ionic TPU), most of the cations and anions of the IL reside in the nanoscale free volume of the TPU film, but intercalation of the ions between the hard segments is also possible.^[34] Consequently, the relative intensity of the XRD peak at 19.3° decreases and a new peak appears at 12.1° , whose relative intensity increases with an increase in the IL content. The peak at 12.1° corresponds to a distance of 7.2 \AA , which matches the dimensions of $[\text{EMIM}]^+$ and $[\text{TFSI}]^-$; this match suggests the intercalation of ions between the hard segments. The XRD pattern of the ionic TPU (80 wt%) well matches that of the ECL TPU (6 wt%), indicating that the small amount of the added luminophore ($[\text{Ru}(\text{bpy})_3][\text{PF}_6]_2$) has only a marginal influence on the entire microstructure of the ECL TPU.

Figure 1f shows SAXS results of $I(q)q^2$ versus q plots for the pristine, ionic, and ECL TPU films, where the presence of a peak at lower q range indicates the inter-domain distance between hard segments within the film.^[35] Incorporation of more IL into the TPU film causes a gradual shift in the peak position toward a smaller q value (from 0.047 to 0.016 \AA^{-1}). This result suggests that the inter-domain distance is gradually expanded in the ionic TPU films with increasing IL content (from 13 to 40 nm). Because the IL occupies the nanoscale free volume around the soft segment domain of the film, loading of more IL will release the entangled soft segments (plasticizer effect) and increase the size of the microscopic domain of the ionic TPU. As is the case with the XRD patterns, the SAXS pattern of the ECL TPU, which includes both the ECL luminophore and the IL, does not show any noticeable differences from that of the composite film containing an equivalent weight fraction of only the IL. These results also support the conclusion that the incorporation of a small amount of luminophore does not cause a noticeable change in the microstructure of the ECL TPU film. The resulting microstructure of the ECL TPU film is schematically depicted in Figure 1g. The ECL

active materials (i.e., luminophore and electrolyte) occupy the nanoscale free volume between the soft segments of the composite and is confined within the TPU network formed by the physical crosslinking of the hard segments. Here, the electrochemical properties of the composite are governed by the included ECL active material, whereas the mechanical properties of the composite are governed by the matrix formed by the TPU network.

The mechanical properties of the ECL TPU film were examined. Figure 2a shows the stress–strain relationship of the ECL

TPU films with different contents (0, 3, 6, 9 wt%) of the ECL luminophore and 80 wt% of IL. Consistent with the structural analysis above, the mechanical response of the ECL TPU film remains nearly unchanged with the amount of ECL luminophore loading. The series of ECL TPU films can be stretched up to 800% (inset in Figure 2a) and their Young's modulus is ≈ 1.2 MPa. We note that such a network polymer composite surrounded by a liquid component can undergo unique mechanical deformation under strain or stress, unlike common solids, liquids, or polymers. For example, when a constant strain is

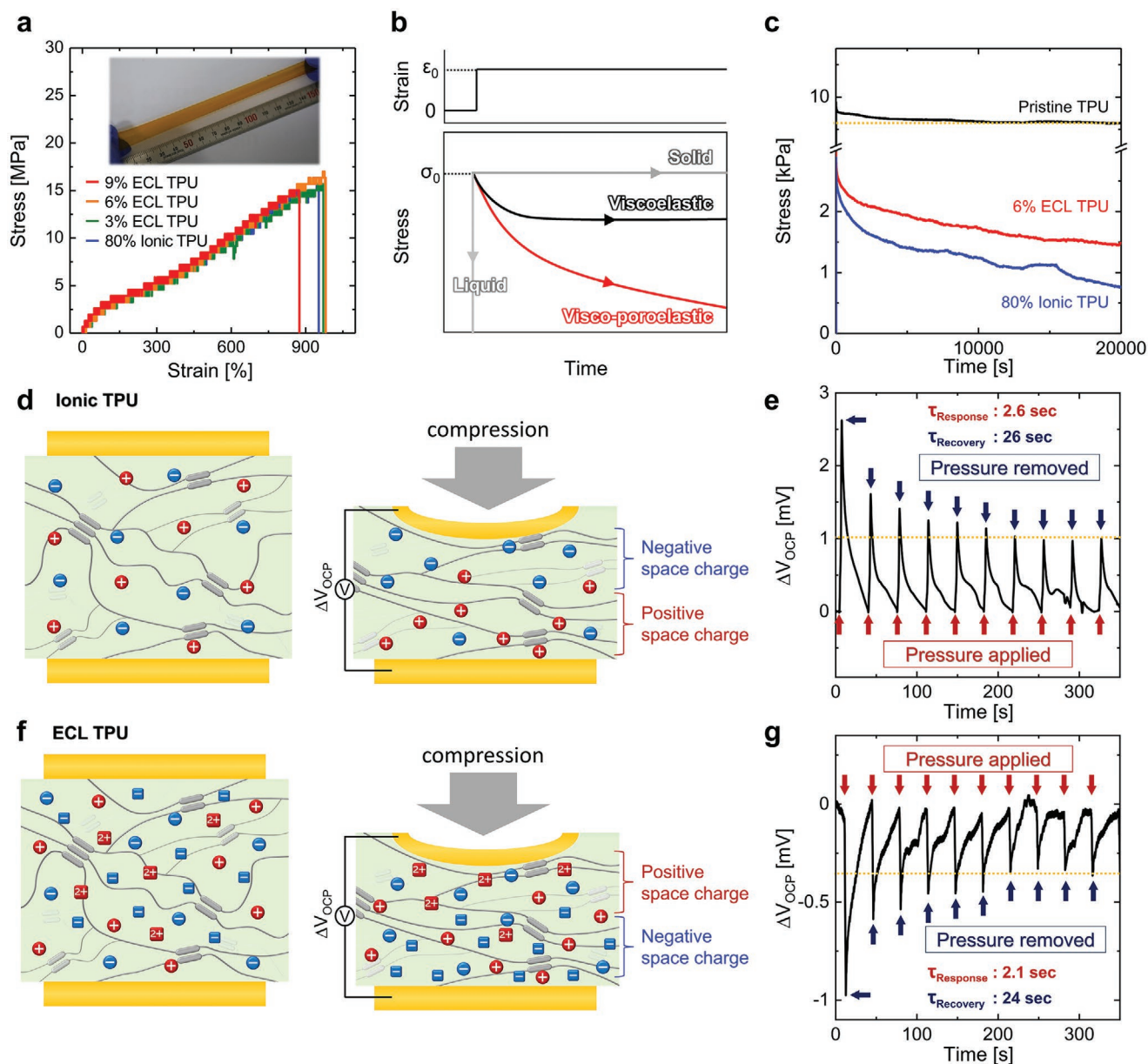


Figure 2. a) Stress–strain relation of ECL TPU films with different loadings of ECL luminophore (0, 3, 6, 9 wt%). The content of IL is fixed to 80 wt% for these films. Inset is a photograph of a stretched ECL TPU film (6 wt%). b) Different stress relaxation behaviors of different types of materials under constant strain. c) Stress relaxation of ECL TPU film (6 wt%), ionic TPU film (80 wt%), and pristine TPU film. d) Distribution of ionic components in an ionic TPU film (left) in equilibrium and (right) under pressure applied on the top. e) Open-circuit potential of an ionic TPU film (80 wt%) recorded under cycles of pressure (10 kPa) application and removal. f) Distribution of ionic components in an ECL TPU film (left) in equilibrium and (right) under pressure applied on the top. g) Open-circuit potential of an ECL TPU film (6 wt%) recorded under cycles of pressure (10 kPa) application and removal.

applied to a solid material, it experiences a constant stress (if the strain is within its elastic regime); however, when a constant strain is applied to a liquid material, it relaxes the mechanical stress immediately by flowing (gray lines in Figure 2b). The behavior of regular polymers lies between those of solids and liquids, which is typically observed in the form of viscoelastic deformation: A fraction of stress is relaxed over a given period of time corresponding to the rearrangement of polymer chains, but after this time taken for molecular rearrangement, the polymer experiences a constant stress, similar to that in common solids (black curve in Figure 2b). Network polymer composites surrounded by a liquid component, for example, our ECL TPU, can show not only viscoelastic deformation behavior by the rearrangement of the polymeric components of the composite itself but also motions of the liquid component by reconstruction of the pore structure, that is, poroelastic behavior.^[36,37] The combination of these two behaviors, known as visco-poroelastic deformation, is a characteristic of such materials, and it leads to a continuous relaxation of stress on a long time scale, even after completion of the viscous response of the polymeric component (red curve in Figure 2b); the visco-poroelastic responses of different materials occur over different periods of time and for different lengths of time.^[38]

The visco-poroelastic behavior of the ECL TPU film (6 wt%) was examined via a time-dependent stress relaxation test. For comparison, the same set of tests was also conducted on both the ionic TPU film (80 wt%) and the pristine TPU film. A step strain of 5% was instantaneously applied to the films and the relaxation of the loaded stress was monitored over a period of time. Figure 2c shows the stress-relaxation behaviors of the pristine (black), ionic (blue), and ECL (red) TPU films. The pristine TPU film showed relaxation behavior typical of a polymeric material, that is, viscoelastic behavior; the stress initially relaxed over a period of time and subsequently attained equilibrium. For both the ECL TPU film and the ionic TPU film, the stress relaxed continuously over an extended period of time (longer than at least 20 000 s). We conjecture that the IL in the ionic TPU and the IL/luminophore mixture in the ECL TPU film were actively involved in the poroelastic relaxation of the composite upon deformation of the pore structure of the network.

Interestingly, the visco-poroelastic deformation of the ECL TPU film leads to a change in the spatial distribution of multiple ionic components within the scaffolding polymer matrix, which we refer as the piezo-ionic effect.^[39,40] The piezo-ionic effect under a load originates from: i) the transient stress distribution built in the visco-poroelastic TPU film (ECL TPU or ionic TPU film) along the normal direction of the applied force, and ii) the different transport capability of the ionic components in the film in response to the built stress distribution (Figure 2d).^[41,42] The more mobile components would escape away from the interface where the force is applied, whereas the less mobile components would remain relatively near the contact.

The piezo-ionic effect could be confirmed by measuring an open-circuit potential (ΔV_{OCP}) between two electrodes placed on top and bottom of the TPU film under pressure.^[30,43] We first discuss the ΔV_{OCP} monitored for the ionic TPU film containing only $[\text{EMIM}]^+$ and $[\text{TFSI}]^-$ without ECL luminophores

(Figure 2e). For the ionic TPU, the piezo-ionic effect is originated from the different mobility as well as different ion-matrix interaction of $[\text{EMIM}]^+$ and $[\text{TFSI}]^-$ within the TPU matrix. The binding energy of the TPU matrix with $[\text{TFSI}]^-$ is estimated to be an order of magnitude stronger than that with $[\text{EMIM}]^+$,^[31,34] therefore, $[\text{EMIM}]^+$ is expected to be more mobile in the TPU matrix than $[\text{TFSI}]^-$. When pressure is applied onto an ionic TPU film from the top, the more mobile ions, that is, $[\text{EMIM}]^+$, will be driven away from top, while leaving the less mobile ions, that is, $[\text{TFSI}]^-$, behind. Consequently, negative and positive space charges can be built across the film. This is reflected to the observation of positive ΔV_{OCP} values upon applying pressure; once the pressure is removed, ΔV_{OCP} will slowly recover its original value until uniform distribution of ions is acquired (Figure 2e).

The piezo-ionic effect is more complicated for ECL TPU films where $[\text{Ru}(\text{bpy})_3]^{2+}$ and $[\text{PF}_6]^-$ are also involved within the TPU matrix in addition to $[\text{EMIM}]^+$ and $[\text{TFSI}]^-$ (Figure 2f). In fact, completely different features in the ΔV_{OCP} profile are acquired upon pressing such that the value of ΔV_{OCP} under pressure is negative, and its magnitude is reduced (Figure 2g). When pressure is applied onto the ECL TPU film from the top, the spatial charge distribution described above for the ionic TPU film would be less apparent (and therefore, the magnitude of ΔV_{OCP} should be smaller), because the positive space charge formed by the least mobile $[\text{Ru}(\text{bpy})_3]^{2+}$ (which would therefore left behind near the top) will negate the negative space charge formed by $[\text{TFSI}]^-$. Moreover, because the valency of $[\text{Ru}(\text{bpy})_3]^{2+}$ is more positive than that of $[\text{EMIM}]^+$, negative ΔV_{OCP} (relative to the bottom electrode) is read from the top electrode. When the applied pressure is removed, the negative ΔV_{OCP} will slowly recover the original value 0, until uniform distribution of ions is reformed. Overall, the apparent difference in the ΔV_{OCP} profiles obtained from the ionic TPU film and the ECL TPU film strongly supports piezo-ionic effect in these films indicating that the distribution of ionic components in the TPU matrix is perturbed when stress is applied.

The piezo-ionic effect of the ECL TPU film could be exploited to assemble the ECL skin device showing characteristic response to mechanical stimuli. Luminescent characteristics of the undeformed ECL skin (6 wt%) were first analyzed. The test device for this analysis was prepared by sandwiching the ECL TPU film between Au and indium tin oxide (ITO) electrodes (see the schematic in Figure 3a). The poor luminescence of the device achieved under a DC bias that arises from the slow migration $[\text{Ru}(\text{bpy})_3]^{1+}$ species generated at the cathode and the $[\text{Ru}(\text{bpy})_3]^{3+}$ species generated at the anode could be avoided by application of AC voltages.^[27] Through the application of AC voltages, both the reduced and the oxidized forms of an ECL luminophore can be generated at the same electrode in a time interval that depends on the AC operating frequency (all devices in this study were driven at 60 Hz) (inset in Figure 3a). The operating frequency-dependent luminescent characteristics is described thoroughly in our previous work.^[32] At a given operating frequency (e.g., 60 Hz), application of a higher AC voltage yielded stronger luminance (Figure 3a). More importantly, an increase in the concentration of the ECL luminophore in the active layer enhanced the luminance of the device (ECL luminophore concentration: red: 3 wt%, black: 6 wt%, and blue:

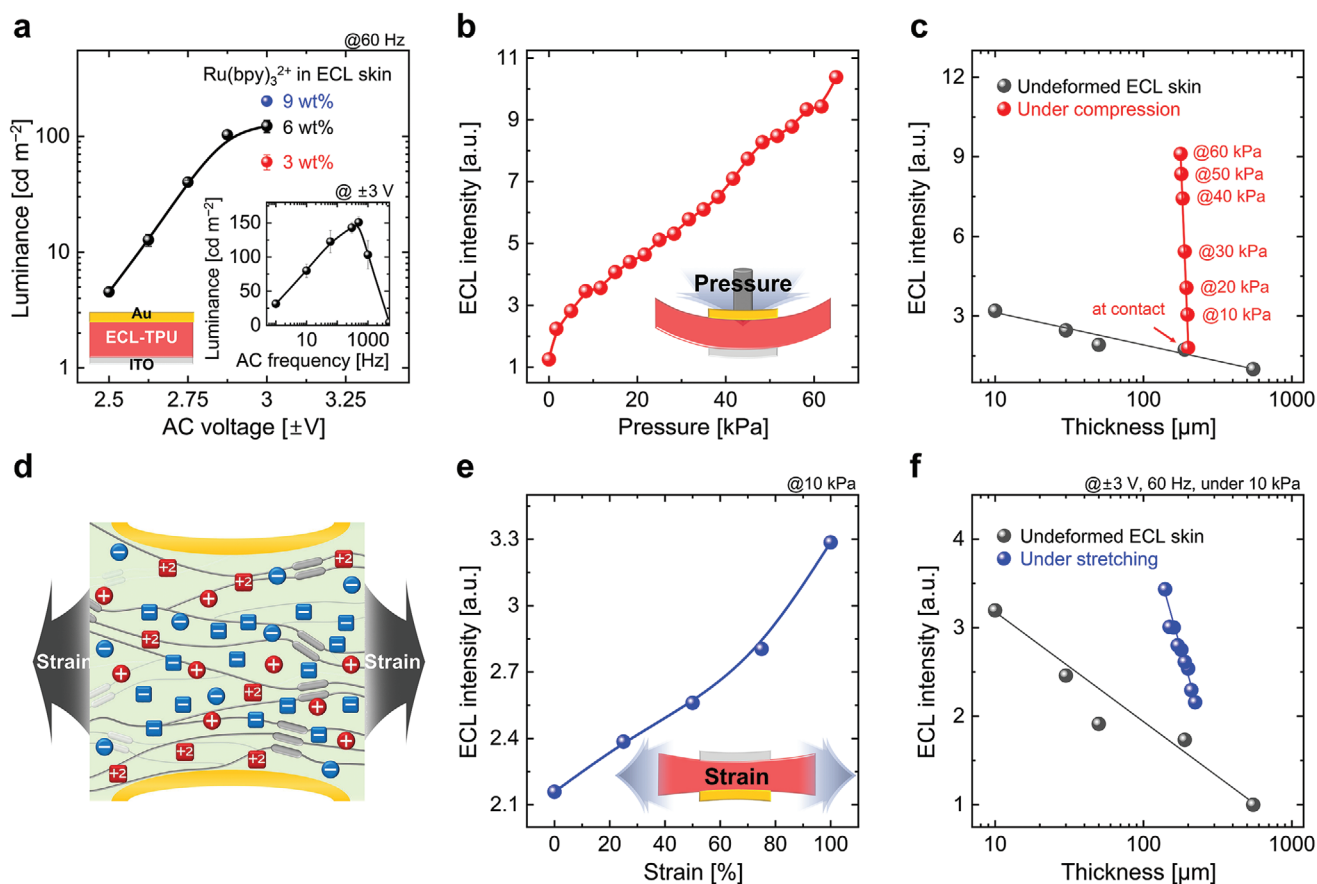


Figure 3. a) Luminance of ECL skin plotted as a function of magnitude of applied AC voltage (at 60 Hz). The inset shows luminance of ECL skin plotted as a function of AC operating frequency (at ±3 V). b) Luminance of ECL skin (200 μm) plotted as a function applied pressure. c) Luminance of ECL skin plotted as a function of thickness of active layer. d) Distribution of ionic components in ECL skin under stretching. e) Change in luminance of ECL skin (223 μm) with applied tensile strain. The data were collected at an AC potential of ±3 V at 60 Hz. The contacting force between the Au electrode and the composite layer was 10 kPa. f) Luminance of ECL skin plotted as a function of active-layer thickness, which was directly measured during tensile test (blue). For comparison, data obtained from undeformed ECL composites with different thicknesses are also plotted (black).

9 wt%). This result is not surprising because for devices with higher luminophore concentration, a larger number of the reactant (i.e., ECL luminophore) would be involved in the redox reactions in the vicinity of the electrodes. We emphasize that this concentration dependence serves as the key source of the stress-dependent luminance of our ECL TPU based on piezoelectric effect described above.

Figure 3b shows the normal-stress-dependent ECL intensity of the AC-driven ECL skin. For this measurement, the ECL composite laminated onto the ITO electrode was pressurized using a force gauge coated with an Au contact (area: 6 mm²) that served as the counter electrode. The variation in the ECL intensity under application of an AC voltage (±3 V at 60 Hz) between the ITO electrode and the Au contact was monitored using a photodiode. With an increase in the applied normal stress up to 60 kPa, the luminance increased approximately eightfold compared with that obtained in the undeformed state. The enhanced luminance was consistently observed upon applying cycles of normal stress (Figure S2, Supporting Information) and upon continuously applying a normal stress (Figure S3, Supporting Information). This eightfold enhancement of the ECL intensity can be attributed to several factors.

The simplest explanation is that the reduced thickness of the active composite layer can cause an increase in the ECL intensity. To examine the influence of the thickness of the active layer on its ECL intensity, we prepared a series of ECL films with the same composition but different thicknesses. Comparison of the ECL intensities of the series of films in their undeformed state under the same operating conditions (±3 V at 60 Hz) revealed the contribution of the thickness variation to the ECL intensity enhancement. As shown in Figure 3c, the results obtained from the undeformed ECL skins with different thicknesses (black points) revealed a thickness-dependent variation in the ECL intensity. The ECL enhancement factor was 1.2; we define this factor as the relative change in the ECL intensity with a decrease in the film thickness by one order of magnitude and express it in the unit of ECL-intensity/dec (this factor can be estimated from the slope of the data). The thickness dependence can be understood from variation in the effective electric potential applied near the electrode. Larger electric field is applied at the electrodes of thinner ECL skins due to the smaller bulk resistance of thinner film (note that the bulk resistance of an electrical system cannot be simply neglected even if a large fraction of the applied potential is compensated

by the formation of electric double layer at interface). However, we emphasize that the thickness variation cannot fully explain the eightfold enhancement of the ECL intensity of our device. The red points in Figure 3c were obtained by re-plotting the black points in Figure 3b; they represent the ECL intensity plotted as a function of the active-layer thickness, which was recorded simultaneously during the ECL intensity measurement. As can be found from the distinct offset in the slope, the ECL enhancement factor is as large as 137 ECL-intensity/dec. This result indicates that a factor more critical than the thickness needs to be considered for explaining the normal-stress dependence. We attribute the enhancement mainly to change in the density of $[\text{Ru}(\text{bpy})_3]^{2+}$ near the electrode/ECL TPU film interface caused by the piezo-ionic effect, recalling that the luminance of an AC-driven ECL device increases with the concentration of luminophore (Figure 3a).

The piezo-ionic effect in the visco-poroelastic ECL TPU layer would be induced not only by normal stress but also by tensile stress. However, the resulting distribution of ions within the visco-poroelastic TPU film under tensile stress would be different from that under normal stress (Figure 3f). Due to the symmetric deformation of the film under stretching, the distributions of ionic components in ECL TPU film should also be symmetric to the central plane of the film, while the effective concentration of $[\text{Ru}(\text{bpy})_3]^{2+}$, that is, the least mobile ionic components, near the surface would be increased (Figure 3d). Accordingly, we examined the ECL intensity of the ECL skin as a function of strain (ϵ). We note that to investigate the inherent contribution of the tensile stress applied to the ECL skin to its ECL intensity, a stretchable electrode that shows negligible variances in the resistance and transmittance over a range of strains is necessary. However, to the best of our knowledge, such an ideal electrode material is not yet available. Therefore, we instead utilized an Au-coated force gauge as an electrode of the device, which can form a direct contact with the ECL TPU layer placed on the ITO electrode. This apparatus was used to perform the measurement, which involved: i) stretching of the composite layer, ii) lamination of the contact to the ECL TPU layer by application of a designated pressure, and iii) recording of the ECL intensity under AC voltage operation. Each time the ECL TPU was to be stretched, the contact had to be removed, and after each instance of stretching of the ECL TPU, the contact was laminated to the film. Unexpected effects of changes in the contact area, sheet resistance, and contact resistance could be prevented by using a nondeformable contact (area: 6 mm²) and setting of the contact pressure. Figure 3e plots the ECL intensity as a function of strain, which was recorded under the condition of formation of a contact at a pressure of 10 kPa (this pressure corresponds to the minimal force required to achieve uniform emission over the contacted ECL skin). As ϵ increased to 100%, the ECL intensity increased by a factor of 1.5, without significant hysteresis. We emphasize that such a positive ϵ -luminance relation can open up new avenues in stretchable optoelectronics; conventional stretchable devices exhibit inferior performance when they are stretched significantly. The origin of the ECL enhancement under stretching cannot be explained simply by the reduced thickness of the ECL skin layer upon stretching. Figure 3f plots the ECL intensity as

a function of the ECL skin layer thickness—which was directly measured during the tensile tests—along with the results obtained for undeformed samples with different thicknesses. The measured ECL enhancement factor upon stretching was 5.6 ECL-intensity/dec, which is larger than the value of 1.2 ECL-intensity/dec in the unstretched state; the higher value in the stretched state reflects the sole dependence of the ECL intensity on the thickness. As also surmised from the results under normal stress, we conjecture that the more critical contributing factor to the ECL enhancement is the increased concentration of $[\text{Ru}(\text{bpy})_3]^{2+}$, that is, the least mobile ionic components, near the ECL TPU/electrode interface.

By exploiting the unique rheological characteristics of the ECL TPU, we fabricated an ECL skin device capable of transducing strain-sensitive, local mechanical stimuli into visual outputs. Figure 4a depicts the structure of the device, which comprises a planar ITO electrode, an ECL skin layer, and copper wire electrodes shaped in alphabetical letters A, B, and C. The device was fabricated simply by laminating the two sides of the ECL TPU film with ITO and copper wire electrodes. With an increase in the normal stress applied to the ECL skin (from 0 to 60 kPa), the emission of the device along the shape of the electrode increased gradually (Figure 4b), which demonstrates the stress-dependent emission of the ECL skin originating from its unique visco-poroelastic response. In addition, when only one of the three letter-shaped copper wires was selectively pressurized to concentrate the stress on this wire, luminescence was concentrated only on this pressurized wire despite all the three letter-shaped wires being connected electrically (Figure 4c). Similarly, when two of the three letter-shaped wires were selectively pressurized, luminescence was observed from underneath both these wires even though electric potential was applied to all three electrodes. These results imply that it is possible to achieve a spatially resolved emission from the ECL skin without any precise efforts directed toward the formation of spatially resolved patterns of the active material.

3. Conclusion

We have demonstrated that a composite comprising a polymer matrix surrounded by liquid ECL active material (a mixture of the luminophore and electrolyte) shows a visco-poroelastic response to mechanical stress leading to change in the distribution of ions inside. We then successfully exploited this characteristic to design a device platform termed ECL skin that transduces mechanical stimuli into visual readout. This device platform is designed simply by sandwiching the composite layer between two electrodes, and it exhibits both normal-stress- and tensile-stress-dependent emissions. Because the mechanical response of the composite can occur locally and induce changes in the distribution of the luminophore over a limited regime, stress locally applied to the ECL skin can be spatially resolved into emission without the use of spatially distributed arrays of pressure sensors. The simple fabrication and unique operation of the ECL skin demonstrated herein are expected to pave the way to new strategies for the design of tactile sensors for human-machine interactive electronic skins.

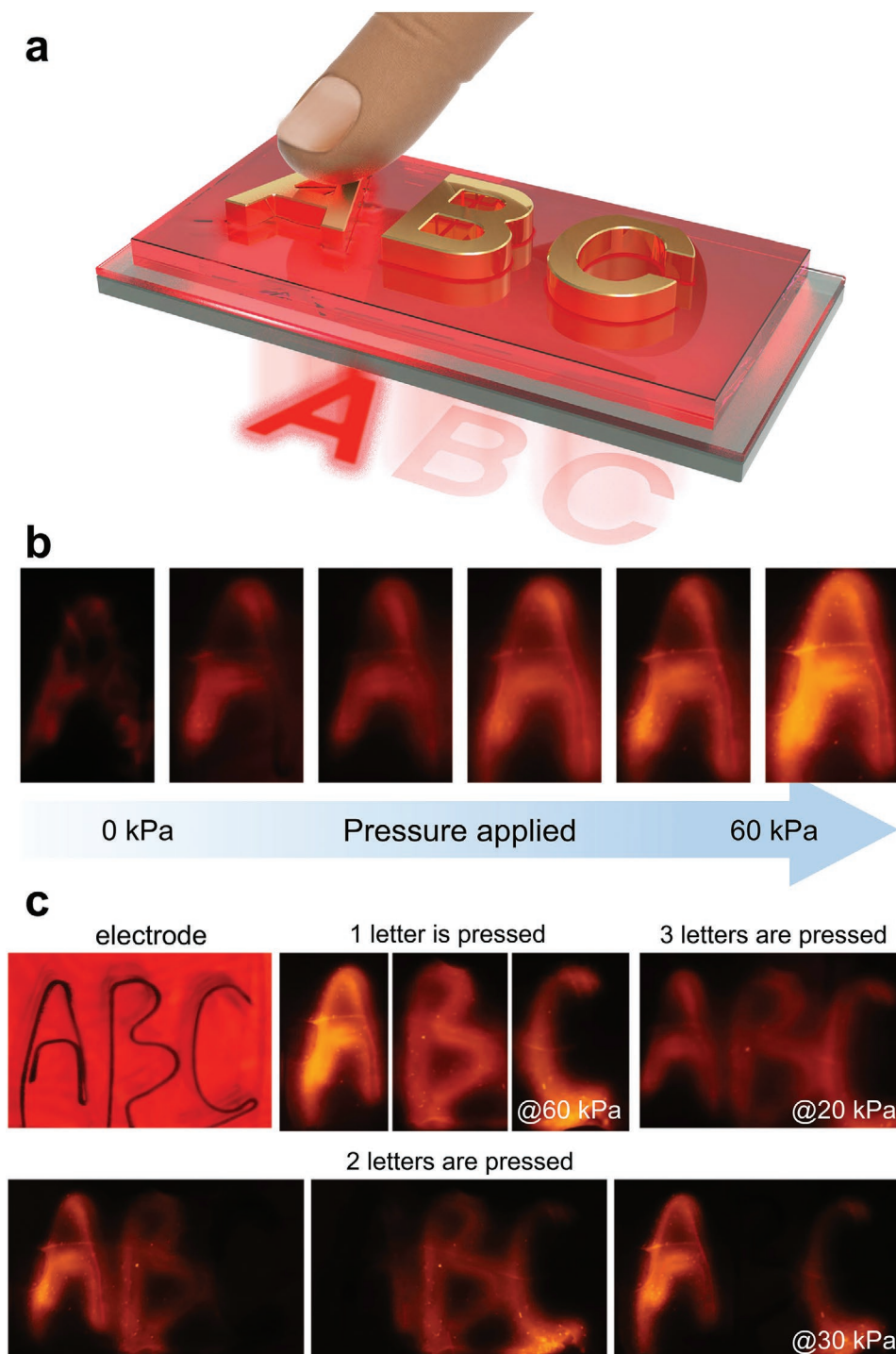


Figure 4. a) Schematic depiction of ECL skin device used for stress-sensitive, local visualization of mechanical stimuli. The photograph shows the copper wire electrodes placed on the ECL skin. b) Series of photographs of ECL skin captured under increase in load applied to electrodes from 0 to 60 kPa. c) Series of photographs of ECL skin captured under various loads selectively applied to one (60 kPa of pressure applied), two (30 kPa of pressure applied), or all three (20 kPa of pressure applied) copper wire electrodes, which were shaped like letters A, B, and C. All photographs were captured at an AC potential of ± 3 V at 10 Hz.

4. Experimental Section

Chemicals and Materials: Tris(2,2'-bipyridine)ruthenium(II) hexafluorophosphate ($[\text{Ru}(\text{bpy})_3][\text{PF}_6]_2$ (97%)) and *N,N*-dimethylformamide (DMF; 99.8% anhydrous) were purchased from

Sigma-Aldrich. TPU pellets were purchased from Kolon Industries, Inc. (product number: KA-480). All these chemicals were stored in a glovebox. 1-ethyl-3-methylimidazolium bis(trifluoromethanesulfonyl) imide ([EMIM][TFSI], high grade) was purchased from C-TRI (Korea). Before use, the IL was stored under vacuum overnight to remove any

residual moisture. Poly(dimethylsiloxane) (PDMS; Sylgard 184) was purchased from Dow Corning Corp. ITO-coated glass substrates (ITO thickness: 1430 ± 100 Å, sheet resistance: $11 \pm 1 \Omega \text{ sq}^{-1}$) were purchased from AMG (Korea). Au/Cr (150/20 nm)-coated PET substrates were prepared by thermal evaporation and cut into slices with dimensions of $1 \text{ mm} \times 6 \text{ mm}$. Before use of these electrode-coated substrates, they were cleaned by ultrasonication in acetone and isopropyl alcohol sequentially for 10 min each; they were then cleaned by UV/O₃ treatment (lamp power: 28 mW cm^{-2} at a wavelength of 254 nm) for 15 min.

Fabrication of Electrochemiluminescence Thermoplastic Polyurethane: As an example, the precursor solution for the ECL TPU containing 6 wt% of the ECL luminophore (relative to the TPU and IL contents) was prepared by dissolving [Ru(bpy)₃][PF₆]₂ (0.5 g) and TPU (2 g) in a mixed solvent consisting of [EMIM][TFSI] (8 g) and DMF (6 g). The weight composition of this precursor solution was [Ru(bpy)₃][PF₆]₂:TPU:[EMIM][TFSI]:DMF = 1:4:16:12 (wt%). Precursor solutions for the ECL skin films with different contents of the ECL luminophore were prepared by the same approach for different weight ratios of [Ru(bpy)₃][PF₆]₂ and [EMIM][TFSI]. The precursor solution was stirred at 80 °C for 12 h. The stirring speed was initially set at 300 rpm but gradually reduced to 60 rpm because the viscosity of the solution increased with the dissolution of TPU. The well-mixed precursor solution was dropped onto the PDMS substrate and spin-coated for 60 s. The PDMS substrate was used for easy separation of the self-standing ECL TPU film formed after spin coating. The film thickness and uniformity could be controlled by altering the rotational speed of the spin coater (50, 200, 500, 1000, and 3000 rpm). The resulting ECL films were placed under vacuum for more than 72 h to completely remove the residual solvent. It should be noted that the residual DMF in the film has a significant impact on the film's luminescence characteristics. Thus, vacuum drying for a long time was critical. The spin-coated ECL film was then cut using a dumbbell cutter and then transferred onto a sample holder using tweezers.

Device Fabrication: The test device in Figure 3a was fabricated in two steps (see Figure S4, Supporting Information). First, a ECL TPU film (prepared separately on a PDMS substrate) was gently laminated onto a glass substrate that was coated with ITO. Subsequently, another glass substrate coated with thin Au layer (thickness 100 nm) was placed on top of the ECL TPU film. The two glass substrates (coated with ITO and Au, respectively) sandwiching the ECL TPU film were gently pressurized by a bulldog clip to form good contact. The luminescence characteristics of the ECL skin under normal pressure (Figure 3b) and tensile strain (Figure 3e) were obtained using a homemade apparatus (see Figure S4, Supporting Information). Here, glass coated with ITO was placed into the holder then the ECL TPU film (prepared separately on a PDMS substrate) was gently laminated onto the ITO-coated glass substrate. Instead of using the Au film coated on glass substrate as it was for Figure 3a, a force gauge directly coated with Au (area = 6 mm^2) was utilized, which could apply pressure in control onto the ECL TPU film. For the tensile-stress-dependent luminescence measurement in Figure 3e, the ECL TPU film had to be stretched up to a designated strain value and then the stretched ECL TPU film was laminated onto the ITO-coated glass substrate. Finally, the Au coated force gauge was gently contacted onto the underlying stretched ECL TPU film. Each time the ECL TPU was to be stretched, the contacts (the ITO underneath and the Au coated force gauge on top) had to be removed. After each instance of stretching of the ECL TPU, the contact was re-laminated to the film.

Supporting Information

Supporting Information is available from the Wiley Online Library or from the author.

Acknowledgements

J.I.L. and H.C. contributed equally to this work. This research was supported by the Basic Science Research Program (2020R1A2C3014237,

2021R1A2C2008332) of the National Research Foundation of Korea (NRF) by the Ministry of Science and ICT.

Conflict of Interest

The authors declare no conflict of interest.

Data Availability Statement

Research data are not shared.

Keywords

electrochemiluminescence, ionic liquids, ionic transition metal complexes, piezo-ionic effect, visco-poroelasticity

Received: January 14, 2021

Revised: April 5, 2021

Published online: June 1, 2021

- [1] A. Chortos, J. Liu, Z. Bao, *Nat. Mater.* **2016**, *15*, 937.
- [2] X. Wang, L. Dong, H. Zhang, R. Yu, C. Pan, Z. L. Wang, *Adv. Sci.* **2015**, *2*, 1500169.
- [3] J. Kang, J. B. H. Tok, Z. Bao, *Nat. Electron.* **2019**, *2*, 144.
- [4] T. Someya, M. Amagai, *Nat. Biotechnol.* **2019**, *37*, 382.
- [5] I. You, D. G. Mackanic, N. Matsuhisa, J. Kang, J. Kwon, L. Beker, J. Mun, W. Suh, T. Y. Kim, J. B. H. Tok, Z. Bao, U. Jeong, *Science* **2020**, *370*, 961.
- [6] Q.-Y. Yan, Y.-W. Shia, D.-Y. Guo, W.-Y. Lee, *Macromol. Res.* **2020**, *28*, 660.
- [7] J. Kim, M. Lee, H. J. Shim, R. Ghaffari, H. R. Cho, D. Son, Y. H. Jung, M. Soh, C. Choi, S. Jung, K. Chu, D. Jeon, S.-T. Lee, J. H. Kim, S. H. Choi, T. Hyeon, D.-H. Kim, *Nat. Commun.* **2014**, *5*, 5747.
- [8] C. M. Boutry, M. Negre, M. Jorda, O. Vardoulis, A. Chortos, O. Khatib, Z. Bao, *Sci. Rob.* **2018**, *3*, eaau6914.
- [9] S. Y. Kim, S. Park, H. W. Park, D. H. Park, Y. Jeong, D. H. Kim, *Adv. Mater.* **2015**, *27*, 4178.
- [10] V. Amoli, J. S. Kim, E. Jee, Y. S. Chung, S. Y. Kim, J. Koo, H. Choi, Y. Kim, D. H. Kim, *Nat. Commun.* **2019**, *10*, 4019.
- [11] C. Wang, D. Hwang, Z. Yu, K. Takei, J. Park, T. Chen, B. Ma, A. Javey, *Nat. Mater.* **2013**, *12*, 899.
- [12] D.-K. Kwon, J.-M. Myoung, *ACS Nano* **2020**, *14*, 8716.
- [13] J. Jang, B. Oh, S. Jo, S. Park, H. S. An, S. Lee, W. H. Cheong, S. Yoo, J.-U. Park, *Adv. Mater. Technol.* **2019**, *4*, 1900082.
- [14] B. Lee, J.-Y. Oh, H. Cho, C. W. Joo, H. Yoon, S. Jeong, E. Oh, J. Byun, H. Kim, S. Lee, J. Seo, C. W. Park, S. Choi, N.-M. Park, S.-Y. Kang, C.-S. Hwang, S.-D. Ahn, J.-I. Lee, Y. Hong, *Nat. Commun.* **2020**, *11*, 663.
- [15] C. Pan, L. Dong, G. Zhu, S. Niu, R. Yu, Q. Yang, Y. Liu, Z. L. Wang, *Nat. Photonics* **2013**, *7*, 752.
- [16] Y. Egami, Y. Hasegawa, Y. Matsuda, T. Ikami, H. Nagai, *Meas. Sci. Technol.* **2020**, *32*, 024003.
- [17] M. Kameda, T. Tabei, K. Nakakita, H. Sakaue, K. Asai, *Meas. Sci. Technol.* **2005**, *16*, 2517.
- [18] J. W. Gregory, K. Asai, M. Kameda, T. Liu, J. P. Sullivan, *J. Aerosp. Eng.* **2008**, *222*, 249.
- [19] X. Y. Wei, X. Wang, S. Y. Kuang, L. Su, H. Y. Li, Y. Wang, C. Pan, Z. L. Wang, G. Zhu, *Adv. Mater.* **2016**, *28*, 6656.
- [20] J. H. Lee, Y. S. Park, S. Cho, I. S. Kang, J. K. Kim, U. Jeong, *Nano Energy* **2018**, *54*, 367.

- [21] C. Larson, B. Peele, S. Li, S. Robinson, M. Totaro, L. Beccai, B. Mazzolai, R. Shepherd, *Science* **2016**, 351, 1071.
- [22] S. Li, B. N. Peele, C. M. Larson, H. Zhao, R. F. Shepherd, *Adv. Mater.* **2016**, 28, 9770.
- [23] Y. Zhang, Y. Fang, J. Li, Q. Zhou, Y. Xiao, K. Zhang, B. Luo, J. Zhou, B. Hu, *ACS Appl. Mater. Interfaces* **2017**, 9, 37493.
- [24] M. Valiadi, D. Iglesias-Rodriguez, *Microorganisms* **2013**, 1, 3.
- [25] E. M. Maldonado, M. I. Latz, *Biol. Bull.* **2007**, 212, 242.
- [26] P. von Dassow, M. I. Latz, *J. Exp. Biol.* **2002**, 205, 2971.
- [27] S. H. Kong, J. I. Lee, S. Kim, M. S. Kang, *ACS Photonics* **2018**, 5, 267.
- [28] K. G. Cho, J. I. Lee, S. Lee, K. Hong, M. S. Kang, K. H. Lee, *Adv. Funct. Mater.* **2020**, 30, 1907936.
- [29] R. D. Costa, E. Ortí, H. J. Bolink, F. Monti, G. Accorsi, N. Armaroli, *Angew. Chem., Int. Ed.* **2012**, 51, 8178.
- [30] S. Mirza, D. Yuta, G. Ettore, F. Meisam, M. Shahriar, N. Sina, M. S. Geoffrey, D. W. M. John, *Proc. SPIE* **2015**, 9430, 943026.
- [31] M. L. Jin, S. Park, J.-S. Kim, S. H. Kwon, S. Zhang, M. S. Yoo, S. Jang, H.-J. Koh, S.-Y. Cho, S. Y. Kim, C. W. Ahn, K. Cho, S. G. Lee, D. H. Kim, H.-T. Jung, *Adv. Mater.* **2018**, 30, 1706851.
- [32] J. I. Lee, D. Kang, S. H. Kong, H. Gim, I.-S. Shin, J. Kim, M. S. Kang, *ACS Appl. Mater. Interfaces* **2018**, 10, 41562.
- [33] H. C. Moon, T. P. Lodge, C. D. Frisbie, *J. Am. Chem. Soc.* **2014**, 136, 3705.
- [34] M. L. Jin, S. Park, Y. Lee, J. H. Lee, J. Chung, J. S. Kim, J.-S. Kim, S. Y. Kim, E. Jee, D. W. Kim, J. W. Chung, S. G. Lee, D. Choi, H.-T. Jung, D. H. Kim, *Adv. Mater.* **2017**, 29, 1605973.
- [35] S. G. Musselman, T. M. Santosusso, J. D. Barnes, L. H. Sperling, *J. Polym. Sci., Part B: Polym. Phys.* **1999**, 37, 2586.
- [36] D. G. T. Strange, T. L. Fletcher, K. Tonsomboon, H. Brawn, X. Zhao, M. L. Oyen, *Appl. Phys. Lett.* **2013**, 102, 031913.
- [37] Y. Hu, Z. Suo, *Acta Mech. Solida Sin.* **2012**, 25, 441.
- [38] Q.-M. Wang, A. C. Mohan, M. L. Oyen, X.-H. Zhao, *Acta Mech. Sin.* **2014**, 30, 20.
- [39] Y. Liu, Y. Hu, J. Zhao, G. Wu, X. Tao, W. Chen, *Small* **2016**, 12, 5074.
- [40] V. Triandafilidi, S. G. Hatzikiriakos, J. Rottler, *Soft Matter* **2018**, 14, 6222.
- [41] H. Ahmadzadeh, B. R. Freedman, B. K. Connizzo, L. J. Soslowsky, V. B. Shenoy, *Acta Biomater.* **2015**, 22, 83.
- [42] X. Wang, W. Hong, *Proc. R. Soc. A* **2012**, 468, 3824.
- [43] S. M. Villa, V. M. Mazzola, T. Santaniello, E. Locatelli, M. Maturi, L. Migliorini, I. Monaco, C. Lenardi, M. C. Franchini, P. Milani, *ACS Macro Lett.* **2019**, 8, 414.